Journal of Hand Surgery Global Online 2 (2020) 277–285

Contents lists available at ScienceDirect

Journal of Hand Surgery Global Online

journal homepage: www.JHSGO.org

Original Research

Analysis of Three-Dimensional Anatomical Variance and Fit of the Distal Radius to Current Volar Locking Plate Designs

Madeline Perrin, MEng, [*] Armin Badre, MD, [§] Nina Suh, MD, [†,§] Emily A. Lalone, PhD [*,†,‡]

[*] Department of Mechanical and Materials Engineering, The University of Western Ontario, London, Canada
[†] Department of Surgery, The University of Western Ontario, London, Canada
[‡] School of Biomedical Engineering, Faculty of Engineering, The University of Western Ontario, London, Canada
[§] Roth–McFarlane Hand and Upper Limb Centre, St. Joseph's Health Care, London, Ontario, Canada

ARTICLE INFO

Article history:
Received for publication May 11, 2020
Accepted in revised form July 15, 2020
Available online August 25, 2020

Key words:
Distal radius
Percent contact
Volar cortical angle
Volar locking plate
Watershed line

ABSTRACT

Purpose: Distal radius fractures are the most common upper-extremity fracture and are increasingly being treated surgically with precontoured volar locking plates. It is not currently known whether existing implant designs are anatomically accurate and whether this has clinical implications. The objective of this study was to determine whether anatomic alignment of the distal radius corresponds accurately to modern volar locking plate designs, including any sex-linked differences in morphology of the distal radius. It was hypothesized that the 2 plates examined would show differences in watershed line (WSL) overlap and that female specimens would have a larger overlap compared with males owing to a decrease in plate-WSL border distances.

Methods: We used 3-dimensional models of 20 cadaver arms (10 female: mean age, 88.7 ± 4.6 years [range, 82–97 years]; and 10 male: mean age, 86 ± 3.6 years [range, 81–91 years]) to create 3-dimensional computed tomography models of the distal radius. Virtual models of 2 common volar plates were created and were used to place the plate virtually onto the distal radii. Outcome measures included the volar cortical angle of the bone and plate, the definition of the WSL subsequently followed by quantitative distance and overlap measures, and percent contact between the plate and the distal radius.

Results: Both sexes showed an decrease (approximately 7°) in average volar cortical angle measure from medial to lateral columns that was statistically significantly smaller on the lateral column (males: 38°; females: 29°) compared with the medial column (males: 45°; females: 36°). Watershed line overlap ranged from 0% to 34.8% with statistically significant differences between sexes. Average border distance for females was 2.7 mm, compared with 3.8 mm for males. Maximum percent contact of 22.0% was observed at a 0.3-mm threshold.

Conclusions: Distal radius fractures are common in elderly female patients, yet clinically available plates have important differences in WSL overlap between sexes, and with minimal contact. Female specimens had more WSL overlap than did males. This indicates the need for volar locking plates to be redesigned to factor in anatomical features of individual patients with a particular focus on sex differences.

Clinical relevance: New plate designs should focus on providing smaller head sizes that are more accurately tailored to the natural contours of the volar distal radius. It is recommended that future studies incorporate expertise from multiple surgeons to diversify and further understand plate placement strategies.

Distal radius fractures (DRF) are the most common upper-extremity fracture, accounting for 15% of all fractures.[1,2] These fractures present through a bimodal population distribution of boys and elderly women.[3] Incidence is most common in pediatrics owing to high-energy traumas and sport, whereas elderly women are at risk for low-energy slips and falls.[4,5]

After a DRF, volar locking plates (VLP) may be used to achieve anatomic alignment. In recent years, the use of VLP has become increasingly popular to obtain rigid fixation.[1,6] Most VLP are

Declaration of interests: No benefits in any form have been received or will be received by the other authors related directly or indirectly to the subject of this article.

Corresponding author: Emily Lalone, PhD, Department of Mechanical and Materials Engineering, The University of Western Ontario, Thompson Engineering Building, Room 353, London, ON, Canada N6A 5B9.
E-mail address: Emily.lalone@uwo.ca (E.A. Lalone).

https://doi.org/10.1016/j.jhsg.2020.07.003

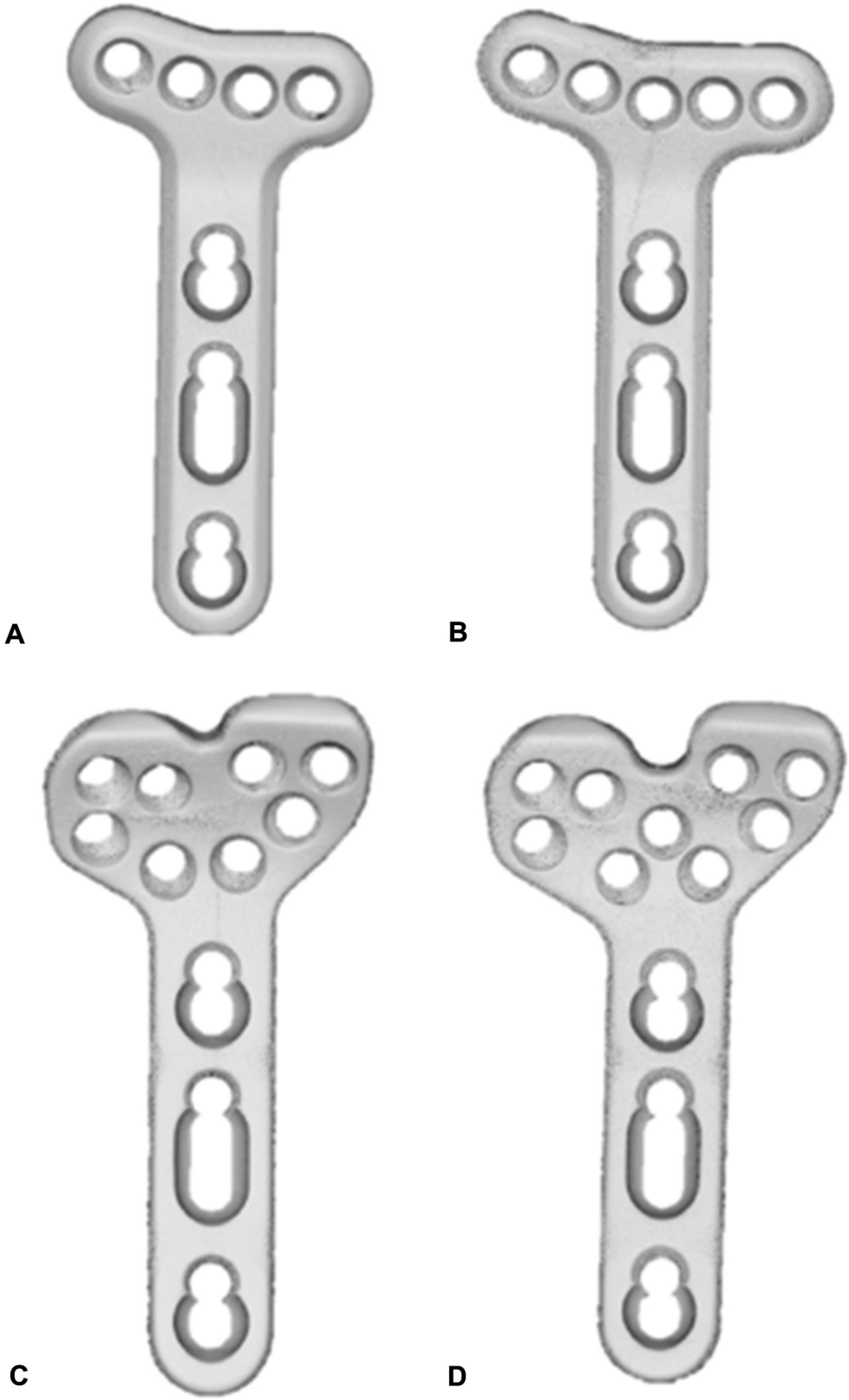

Figure 1. The selected plates included the 2.4-mm LCP volar extra-articular (EA) distal radius plate and the 2.4-mm LCP volar column (VC) distal radius plate (DePuy Synthes). Four-hole small head. **A** 2.4-mm LCP volar EA distal radius plate: four-hole large head. **B** 2.4-mm LCP volar EA distal radius plate: five-hole large head. **C** 2.4-mm LCP VC distal radius plate: eight-hole small head. **D** 2.4-mm LCP VC distal radius plate: nine-hole large head.

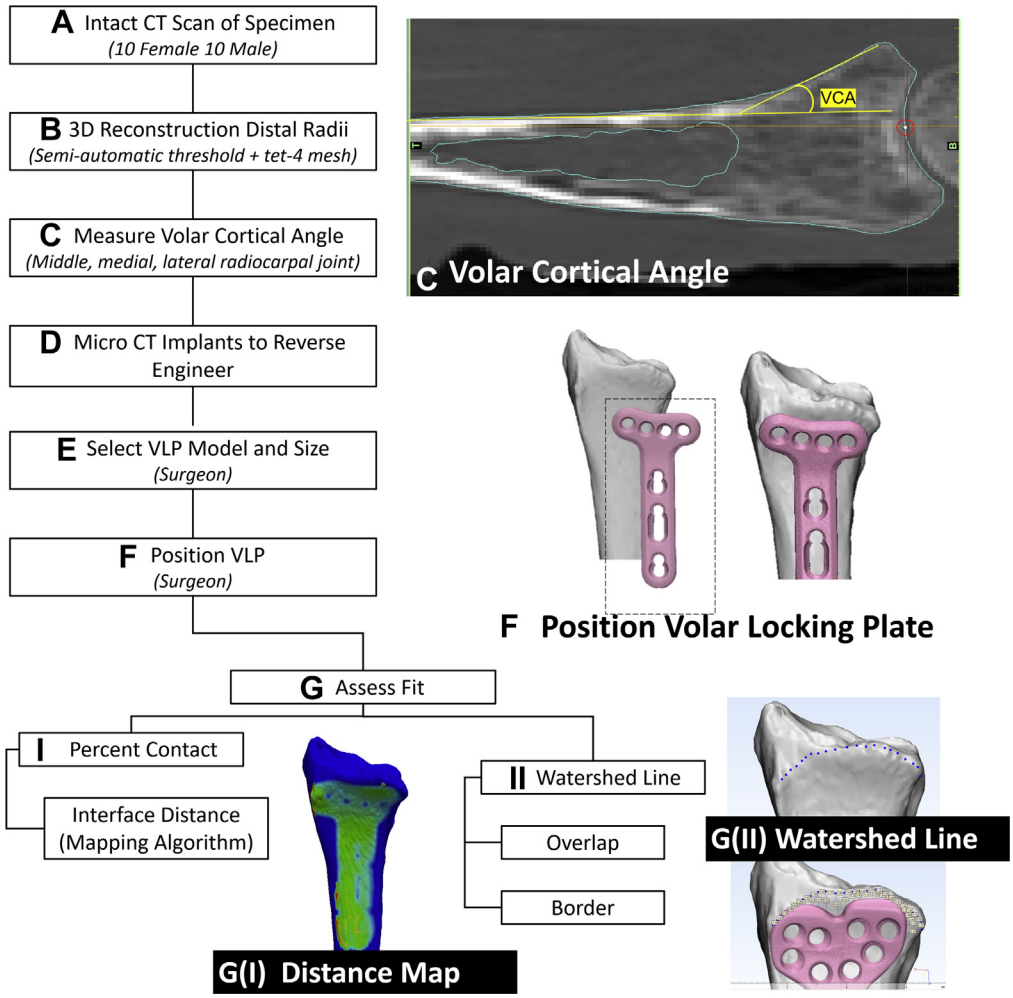

Figure 2. Experimental and data analysis protocol. **A** Computed tomography scan of intact specimen. **B** Three-dimensional (3D) reconstruction of distal radii using Materialize Software Suite. **C** Measurement of VCA using 3 landmarks on radiocarpal joint. **D** Micro-CT 4 implants to reverse engineer models. **E** Selection of VLP model and size by surgeon. **F** Positioning of plate on bone model by surgeon. **G** Assessment of fit categorized by (I) percent contact distance mapping algorithm and (II) WSL border and overlap.

precontoured to incorporate a volar cortical angle (VCA) of 25° across the entire width of the plate.[7] The VCA describes the angle subtended between the volar lip and the shaft of the distal radius. Previous anatomic studies determined that the geometry of the distal radii is complex and that this VCA is inconsistent across the volar surface of the distal radius (medial to lateral).[8–10] In addition, despite the benefits of volar plating technique compared with dorsal approaches, the need and indications for the removal of VLP after bony healing are still controversial.[11] Yamamoto et al[11] conducted a literature review of VLP removal after DRF and found a mean removal rate of 9% overall for all countries. Removal in France, Norway, Japan, and Belgium was as high as 19%, whereas the United States had a low rate of 3%. Previous studies indicated that the risk for tendon rupture is highest in patients in whom the plate is placed directly on or distal to the watershed line (WSL) and that implant plate removal is higher in patients with prominent hardware.[12–15] The nonanatomic nature of some plate designs may contribute to plate prominence, leading to these complications.

The objectives of this study were to (1) assess the anatomical geometry of the distal radius; (2) identify the WSL and determine the effect of plate selection and placement on the distance and overlap of the distal volar edge of the plate to the WSL; and (3) determine the effect of plate selection and placement on the restoration of anatomical alignment by assessing the percent contact between the plate and bone surfaces. We hypothesized that (1) if posterior surface contours of the plates were not matched to the VCA measures of the bones, there would be an increase in WSL overlap and a decrease in percent contact between the surfaces; (2) extra-articular (EA) plates would show less WSL overlap than volar column (VC) plates owing to differences in plate design; and (3) female specimens have considerably more overlap of plates to their WSLs because of a decrease in border distances and petite anatomical features compared with their male counterparts.

Materials and Methods

Specimens

Ten female cadaver specimens (mean age, 88.7 ± 4.6 years; range, 82–97 years) sectioned midhumerus (4 full arms, 6 hand to elbow) and 10 male cadaver specimens (mean age, 86 ± 3.6 years; range, 81–91 years) (8 full arms, 2 hand to elbow) were scanned using a 64-slice computed tomography (CT) scanner (GE Discovery CT750 HD or GE LightSpeed VCT, Waukesha, WI). We chose specimens with minimal radiographic evidence of arthritis, fracture, and deformity. Slices acquired ranged from 305 to 1,286 for each scan (depending on whether the cadaveric specimen was shoulder to fingertips or elbow to fingertips) with a consistent 512 × 512-pixel reconstruction matrix.

Volar locking plates

We chose 2 VLP types for this study because they represent the volar plates that are available at our tertiary care hand and upper limb center and are used to treat 90% of DRF (>4,000/y). The implants themselves were taken from the operating room and CT scanned to obtain the geometry; therefore, they are representative of what would be used to treat most fractures in our practice. The selected plates included the 2.4-mm LCP volar EA distal radius plate and the 2.4-mm LCP VC distal radius plate (DePuy Synthes, Raynham, MA). For each design, 2 distal head sizes were selected. The shortest plate shaft length was chosen for each plate (Fig. 1).

Plates were scanned using a Nikon X/T H 225 ST micro-CT scanner (Nikon, Tokyo, Japan). Slices acquired ranged from 1,842 to 1,936 for each scan with 0.027-pixel spacing and reconstruction matrix ranging from 763 × 1,282 to 1,001 × 1,137.

Three-dimensional models

The CT images for specimens were imported in Digital Imaging and Communications in Medicine (DICOM) format to Mimics Research software (version 21.0, Materialise, Leuven, Belgium) to construct of 3-dimensional models. Model renderings of specimens required segmentation of the radius from surrounding tissues, which was completed using a semiautomatic thresholding technique with predetermined values for bone of 226 to 2,605 Hounsfield units. The long axis of the center of the radial bone was taken to be the reslice origin.

Micro-CT images for VLPs were imported in DICOM format to Mimics Research software to construct of 3-dimensional models. Three-dimensional model rendering of VLPs required thresholding from surroundings to reduce or remove noise and was conducted using a manual thresholding technique. The long axis of the shaft was taken to be the reslice origin. Three-dimensional models of specimens and plates were imported to 3-matic Research software (version 13.0, Materialise) for surface and volume meshing. The partial volume effect of medical imaging is a phenomenon in which a single voxel may contain multiple types of tissue owing to the finite special resolution of the imaging method. To minimize this effect, a maximum edge length of 0.5 × pixel spacing was selected for each individual model.

Plate placement

After 3-dimensional model rendering, plates were placed onto the different distal radius models by a fellowship-trained orthopedic hand surgeon and then verified by a second surgeon using 3-matic Research software. The surgeon placed the EA and VC plates separately on all specimens. The choice was given of the small or large head size for each plate. Manual manipulation was achieved using translation and rotation functions to alter the plate frame of reference to reside on the bone based on visual inspection. For the EA plate design, the goal was to avoid the WSL (no overlap for these plates). Placement concluded with a total of 20 specimens (10 female and 10 male), each with 2 plates placed, for a total of 40 samples.

Measurements

Volar cortical angle

After the initial 3-dimensional volume rendering in Mimics Research, the model was resliced down the longitudinal axis of the bone. Three points were placed for reference on the radiocarpal joint surface according to the methods presented by Evans et al[7] and Gray et al.[16] The reference points correspond to the center of the scaphoid fossa, medial side of the scaphoid fossa, and lateral lunate fossa. Together, these points represent measurement locations for medial, middle, and lateral distal radius VCA measures.

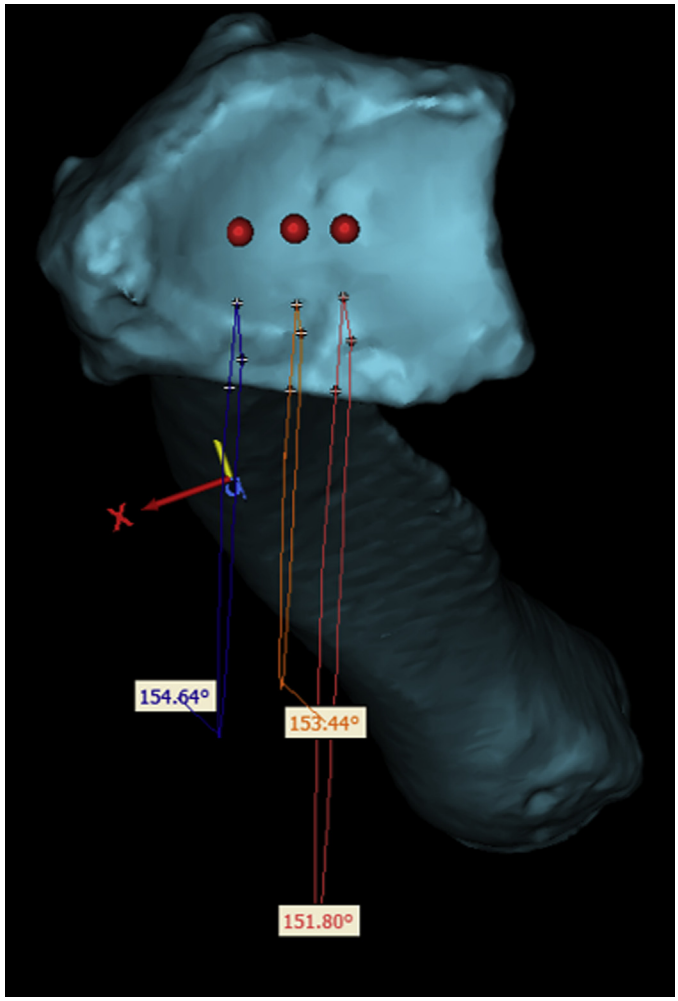

Figure 3. Three-dimensional representation of 3 columnar landmarks on radiocarpal joint surface with corresponding VCA measures (center of the scaphoid fossa, medial side of scaphoid fossa, and lateral lunate fossa).

Locating each point within the sagittal plane of DICOM slices, the contour of the generated model was outlined for reference purposes. The VCA was measured using a 3-point angular measuring tool (Fig. 2C). Figure 3 shows the 3 columnar landmarks on the radiocarpal joint surface with corresponding VCA measures. The 3 points corresponded to (1) the anterior surface of the long axis of the radius, (2) the vertex of the volar radius concave surface, and (3) the anterior prominence of the volar ridge. The vertex was manipulated to provide maximum contact along the length of the shaft and the volar cortex arms of measurement. The process was repeated for each of the 3 reference points and for all specimens.

Watershed line identification

After plate placement in 3-matic Research software, the point and line tools were used to define the WSL of the bone by temporarily hiding the plate from view. The WSL is characterized by a protuberance on the distal volar surface of the radius and is conceptualized as the promontory of the radius. This line can easily be visualized as the most distal line on the radius; as such, it acts as a surgical landmark for implant placement.[17] Using a manual technique, the WSL was identified with primary reference to the

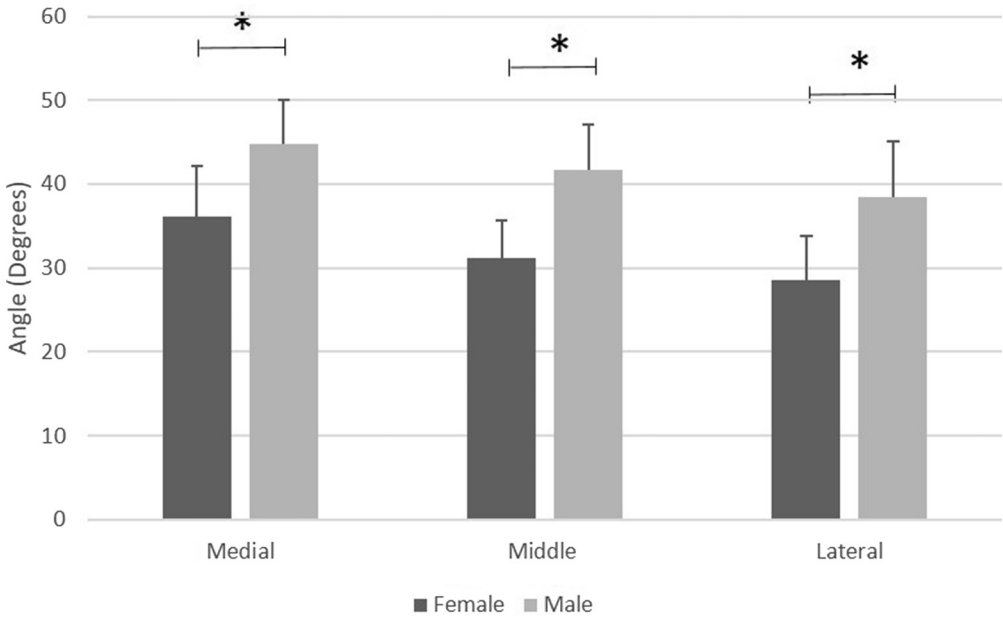

Figure 4. Volar cortical angle. Comparison of inherent VCA of the distal radii among medial, middle, and lateral columnar regions of both males and females. Statistically significant difference is shown between sexes at each columnar region.

identification methods of Imatani et al.[18] Point placement was limited by the software, in which points were able to be placed only at nodes of the surface mesh. Care was taken to maintain equal distances between point selection, while positioning the plate in the desired location (Fig. 2G[II]). The length of the WSL was determined by measuring the distances between all identified WSL points.

Watershed line overlap and border distance

The overlap of the plate to the WSL was determined by visualizing the plate in the coronal view and measuring the length of WSL overlapped by the positioned plate. A continuity of measurement technique based on the nodal method of identifying the length of the WSL was used as noted earlier (Fig. 2G[II]). The percent overlap was calculated by dividing the overlap length by the total WSL length. Finally, the WSL border distance was defined by taking the average distance between the nodes on the WSL and the back of the plate in a perpendicular manner. The border distance therefore describes the distal distance between the WSL and the contoured distal ridge of the VLP after placement and reflects the mismatch between plate design and anatomy creating a prominence.

Percent contact

We measured percent contact between the plate and bone using a custom distance-mapping algorithm developed by Lalone et al.[19] The software, which was written with the Visualization Toolkit, calculated intermodel distances using a nearest point-to-point distance algorithm for points corresponding to vertices within each triangular surface mesh. In principle, the algorithm lists the Cartesian coordinates on both surfaces and assigns a location ID number. A function within the Visualization Toolkit (FindPoint) assigns ID numbers to each point based on (x, y, z) of the point within the model coordinate system. Two points with the same coordinates will have identical ID numbers, and therefore a distance of 0 will return. Nonzero values are displayed using the ID values to determine point proximity and examine differences. For visualization, distances were mapped based on a color-distance assigning method (Fig. 2G[I]). Results were placed into 4 thresholds of plate–bone distances defined as contact to understand the mapping colorization better. Threshold levels include 0, ±0.1, ±0.2, and ±0.3 mm.

Statistical analysis

Outcome variables in this study included the VCA, border distance (in millimeters), watershed overlap (percentage), and percent contact between plate and bone (percentage). Paired *t* tests were conducted for (1) the VCA (3 points for each specimen for both male and female populations), (2) the watershed border (both plate types and both sexes), and (3) watershed overlap (both plate types and both sexes) (either equal or unequal variance assignment, based on F tests). For the VCA measure, we used the paired *t* test to compare angles between males and females for the medial, middle, and lateral points (paired in this way). A 2-way analysis of variance was conducted on percent contact thresholds at all levels between both sex and plate populations. Statistical significance for all data was set at $P < .05$.

Results

The VCA measures were statistically significantly different between sexes at all 3 columnar locations ($P < .01$) (Fig. 4). The female population had average VCA measures of 36.1, 31.1, and 28.6, decreasing from the medial to lateral columns. Although the male population followed that trend, the average VCAs were significantly higher at 44.8, 41.7, and 38.4. Both sexes showed an decrease in average VCA measure from medial to lateral columns that was statistically significantly smaller on the lateral column. Results showed a wide range of overlap percentages distributed across the male/female and E /VC sample groups. Among all groups, across the 40 samples, a range of 0% to 34.7% overlap was observed; 23 of 40 total specimens had no overlap. Of the 23 with no overlap; 9 were female and 14 were male; 12 were EA plate and 11 were VC. The other 17 that had overlap included 9 EA plates (2 males and 6 females) and 9 VC plates (4 males and 5 females). Of the nonzero values, a range of 1.4% to 34.7% was shown. Comparing quantitative averages of specimens with overlap, males had average overlap of 3.3% and 5.5% for EA and

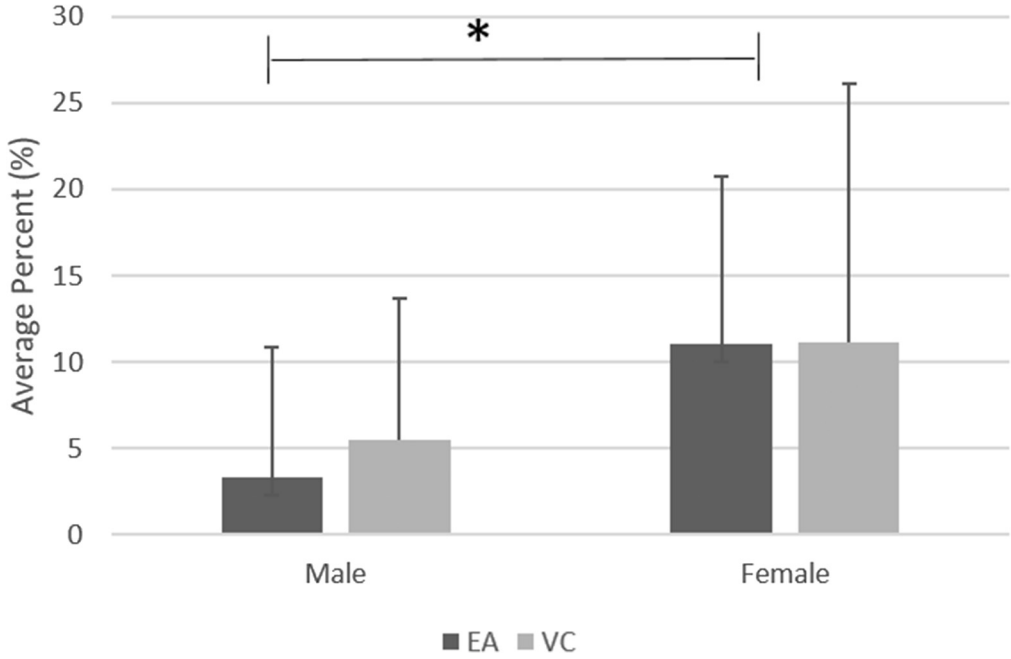

Figure 5. Watershed line overlap. Comparison of overlap of EA and VC VLP with identified WSL. Statistically significant difference is shown only between sexes.

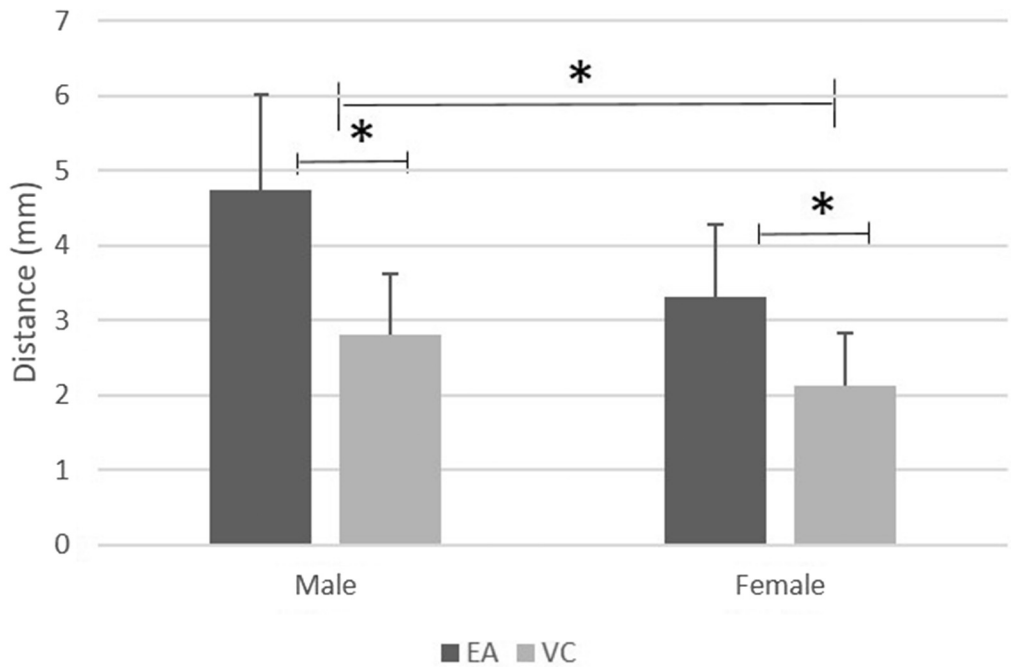

Figure 6. Watershed line to plate border distance. Comparison of border distance maintained between distal edge of EA and VC VLP and identified WSL. Statistically significant difference is shown between both sexes and plates.

VC plates, respectively, whereas average values of 11.0% and 11.1% were observed for females (Fig. 5). There was a statistically significant difference in measurements between specimens; however, this was not the case between plate groups for nonzero and zero values (male/female, $P = .048$; EA/VC, $P = .74$).

We measured the border distance between the WSL and the most distal posterior surface of the plate. The average border distance for all female samples across both plate types was 2.7 mm, compared with a distance of 3.8 mm for males. This corresponds to 39.0% more space on average between the WSL and the distal-posterior surface of the plate for males. Looking at the 2 plate types separately, the EA plate had a larger border distance in both the male and female populations, with a distance on average of 4.7 and 3.3 mm accordingly (Fig. 6). This corresponded to males having an average of 43.3% (1.4-mm) larger border distance than that of females with the EA plate type. For VC plates, the average distance was 2.8 mm for males and 2.1 mm for females. In comparison, males had an average of a 31.7% (0.7-mm) larger border distance. Statistically significant differences were shown between different sexes and plate types (male/female, $P = .01$; EA/VC, $P = .001$).

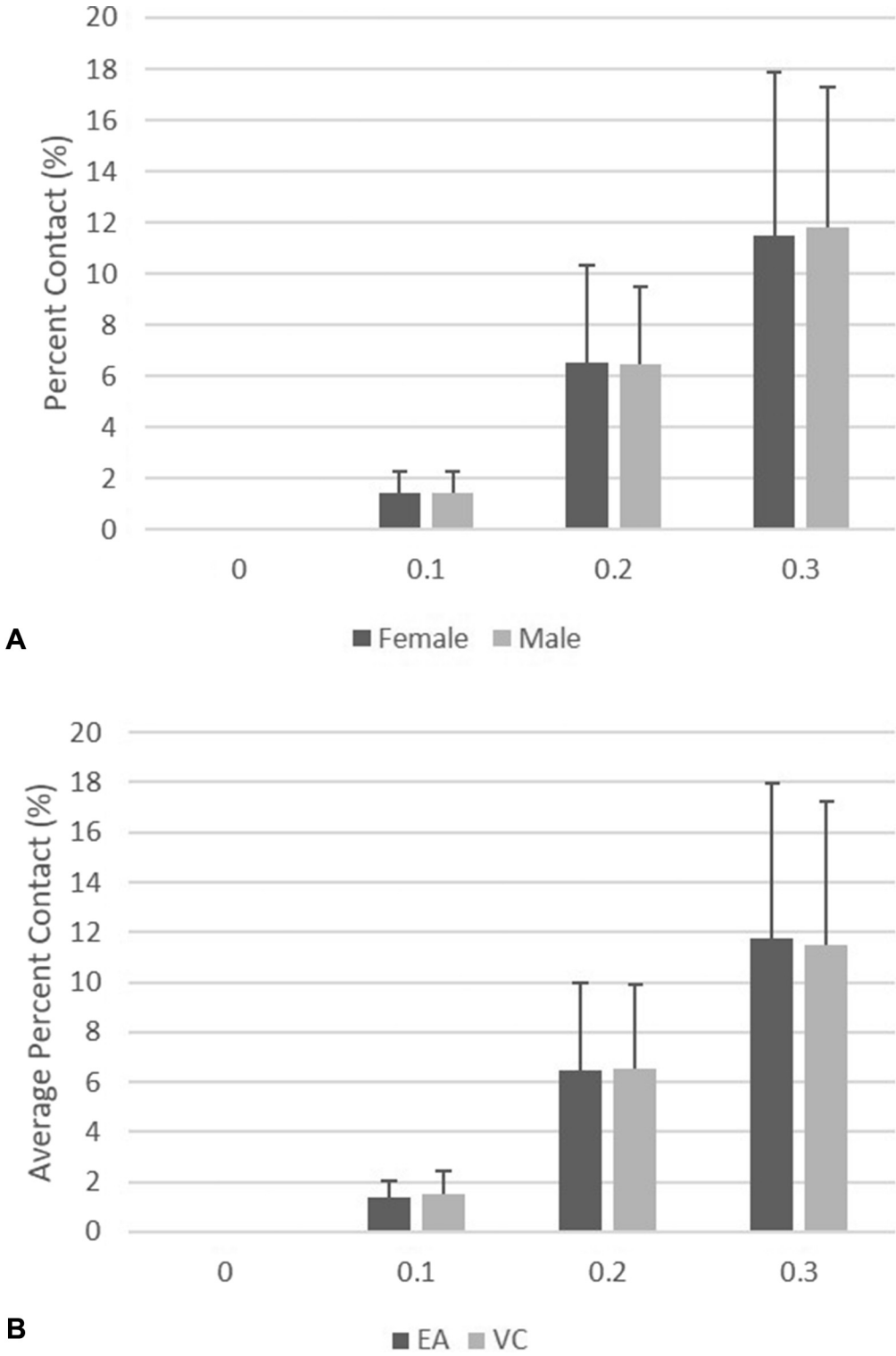

Figure 7. Percent contact. Watershed comparison of average percent contact between **A** sex populations and **B** plate populations at 4 threshold levels (0, 0.1, 0.2, and 0.3 mm). There were no statistically significant differences between sexes or plate types for any threshold level.

Results after the use of the distance mapping algorithm showed no points on any of the 40 samples that exhibited contact at the 0-mm threshold. Essentially, there was no perfect contact between the posterior plate surface and the anterior bone surface.

For the percent contact, 4 thresholds of plate–bone distances were measured and compared (0, ±0.1, ±0.2, and ±0.3 mm), but they showed no statistical significance at any level (0.1 mm, $P = .97$; 0.2 mm, $P = .95$; and 0.3 mm, $P = .86$) (Fig. 7). When we analyzed all individual specimens, we observed a maximum percent contact of 21.97% in specimen F4 at a 0.3-mm threshold.

Upon comparison of the percent contact difference between EA and VC plates, there was no statistically significant difference between the EA and VC populations (0.1 mm, $P = .61$; 0.2 mm, $P = .93$; and 0.3 mm, $P = .91$). Furthermore, a 2-way analysis of variance for

each threshold level between male/female and EA/VC populations showed no statistically significant difference among samples, columns, or interactions.

Discussion

This study investigated incoherency between the VCA of the distal radius and the precontoured angle of VLP. We hypothesized that if the VCA measures between plate and bone were unequal, there would be an increase in WSL overlap and a decrease in percent contact between the surfaces. Our results agreed with the literature, indicating that the VCA of bone was larger than that of the EA and VC precontoured plates examined in this study.[3,7,20] Female specimens had smaller VCA measures than did males. Both the male and female populations also had a distinct pattern in relation to the columnar theory of the radius.[21] From the medial to lateral side of the bone, the VCA increased for all specimens. The VCA of the distal radius varies between sexes and does not follow the same degree within the mediolateral direction. This finding agrees with the theory presented by Oppermann et al [22] in 2015, in which the distal ulna and distal radius form a 3-column biomechanical construct. The 2 bones are divided into 3 columns according to medial, intermediate, and lateral locations. This construct has maintained wide acceptance in the current literature.[21,22]

The percent overlap of plate to WSL was relatively subjective in nature. However, results showed statistically significant differences between sexes, but not for plate type. Therefore, regardless of the plate type used, female WSL are more often overlapped or covered compared with their male counterparts. The data presented were widely spread; more than 50% of the total specimen population showed no overlap. The remaining specimens ranged from 1.44% to 34.76% overlap, and the highest overlap was for a female VC placement. The hypothesis of this outcome measure was that the EA plate would show a lower overlap compared with VC owing to the differences in plate design. It was also anticipated that the female specimens would have notably more overlap owing to the decrease in border distance.

In quantitatively assessing the WSL border distance, we found that males maintained an average of 43.3% (1.4-mm) larger border distance than did females for the EA plate and a 31.7% (0.68-mm) larger border distance for the VC plate. Statistical analysis showed significant differences between sexes and plate types; females and VC plates exhibited smaller border distances. For VC plates, this is an inherent feature of the design of the plate and its specifications for fracture patterns. The EA plate is designed to be placed more proximal, away from the WSL, for treatment of more simple fractures such as Colles and Smith types with little fragmentation.[5] On the other hand, VC plates are designed to be placed more distal, in close proximity to the WSL. The curvature of the plate head is designed for additional bony screw purchase of fragments and intra-articular fracture patterns. The border distances for the EA plates were significantly larger for both males and females compared with the VC plates.

A previously developed distance-mapping algorithm was used to analyze percent contact between the volar-anterior distal radius and the posterior-VLP surface. From limited findings in previous studies, the most comparable results were those of Buzzell et al,[20] who reported a contact range of 3% to 6% using pressure films. Whereas that study physically manipulated 2 rigid surfaces, the outcome measure was primarily a function of the pressure applied in contact. The technique used in the current study, although computational in nature, relied on plate placement from surgical consultants. The technique of Buzzell et al did not use any type of fellowship-trained technician.

It is well-established that the fracture pattern and fragmentation affect the type of plate and placement that surgeons select *in vivo*. Inherently, the 2 different styles of plates selected for this study, EA and VC, are used for 2 different fracture patterns. One limitation of this study was that we did not have a simulated bone fracture that was being fixated. To overcome this, the surgeon was asked to place both an EA and a VC plate on each specimen; however, the software did not have the ability to set boundary conditions. This allowed the plate to be placed inside the bone, or proud on top of the bone. In addition, the WSL was identified manually and therefore was highly subjective. Manual techniques relied on using the mesh nodes, which were a function of the maximum mesh edge length determined from DICOM data to minimize partial volume effects. Watershed line points were able to be selected only at these node points, because each mesh size was a function of individual scan parameters.

This study explored a number of techniques that, to the authors' knowledge, were not previously presented in the literature, such as the distance-mapping algorithm and 3-dimensional plate placement. In addition, a previously presented method for columnar VCA measures was used.[16] Overall, the implications of this study are expected to empower the development of new plate designs.

This study shows that neither EA nor VC plates currently provide an adequate sizing solution for female patients. Female specimens had smaller VCA angles, which, combined with small border distances, presents a valid case for the redesign of VLP. New designs should focus on providing smaller sizes of the distal row of the plates or more modular implant components that are more accurately tailored to the natural contours of the volar distal radius. It is recommended that future research studies incorporate expertise from multiple surgeons to diversify and further understand plate placement strategies. To eliminate study limitations, the functionality of the software employed for placement should include boundary condition settings to remove the likelihood of plates being placed inside the bone. It may also be a viable alternative to place a plate physically onto the cadaver specimens before CT scanning. Finally, modeling strategies should be developed to understand and quantify the effect of distal plate prominence on the likelihood of tendon complications.

References

1. Nana AD, Joshi A, Lichtman DM. Plating of the distal radius. *J Am Acad Orthop Surg*. 2005;13(3):159–171.
2. Larsen CF, Lauritsen J. Epidemiology of acute wrist trauma. *Int J Epidemiol*. 1993;22(5):911–916.
3. Obert L, Loisel F, Gasse N, Lepage D. Distal radius anatomy applied to the treatment of wrist fractures by plate: a review of recent literature. *SICOT J*. 2015;1:14.
4. Beleckas C, Calfee R. Distal radius fractures in the athlete. *Curr Rev Musculoskelet Med*. 2017;10(1):62–71.
5. Blakeney W. Stabilization and treatment of Colles' fractures in elderly patients. *Clin Interv Aging*. 2010;5:337–344.
6. Drobetz H, Schueller M, Tschegg EK, Heal C, Redl H, Muller R. Influence of screw diameter and number on reduction loss after plating of distal radius fractures. *ANZ J Surg*. 2011;81(1–2):46–51.
7. Evans S, Ramasamy A, Deshmukh SC. Distal volar radial plates: how anatomical are they? *Orthop Traumatol Surg Res*. 2014;100(3):293–295.
8. Lewis OJ, Hamshere RJ, Bucknill TM. The anatomy of the wrist joint. *J Anat*. 1970;106(part 3):539–552.
9. McCann PA, Clarke D, Amirfeyz R, Bhatia R. The cadaveric anatomy of the distal radius: implications for the use of volar plates. *Ann R Coll Surg Engl*. 2012;94(2):116–120.
10. McCann PA, Amirfeyz R, Wakeley C, Bhatia R. The volar anatomy of the distal radius—An MRI Study of the FCR approach. *Injury*. 2010;41(10):1012–1014.
11. Yamamoto M, Fujihara Y, Fujihara N, Hirata H. A systematic review of volar locking plate removal after distal radius fracture. *Injury*. 2017;48(12):2650–2656.

12. Lutsky KF, Beredjiklian PK, Hioe S, Bilello J, Kim N, Matzon JL. Incidence of hardware removal following volar plate fixation of distal radius fracture. *J Hand Surg Am*. 2015;40(12):2410–2415.
13. Kitay A, Swanstrom M, Schreiber JJ, et al. Volar plate position and flexor tendon rupture following distal radius fracture fixation. *J Hand Surg Am*. 2013;38(6):1091–1096.
14. Soong M, Earp BE, Bishop G, Leung A, Blazar P. Volar locking plate implant prominence and flexor tendon rupture. *J Bone Jointt Surg Am*. 2011;93(4):328–335.
15. Agnew SP, Ljungquist KL, Huang JI. Danger zones for flexor tendons in volar plating of distal radius fractures. *J Hand Surg Am*. 2015;40(6):1102–1105.
16. Gray RJ, Thom M, Riddle M, Suh N, Burkhart T, Lalone E. Image-based comparison between the bilateral symmetry of the distal radii through established measures. *J Hand Surg Am*. 2019;44(11):966–972.
17. Windisch G, Grechenig W, Peicha G, Tesch NP, Seibert FJ. Capsular attachment to the distal radius for extracapsular placement of pins. *Surg Radiol Anat*. 2001;23(5):313–316.
18. Imatani J, Akita K, Yamaguchi K, Shimizu H, Kondou H, Ozaki T. An anatomical study of the watershed line on the volar, distal aspect of the radius: implications for plate placement and avoidance of tendon ruptures. *J Hand Surg Am*. 2012;37(8):1550–1554.
19. Lalone EA, McDonald CP, Ferreira LM, Peters TM, King GW, Johnson JA. Development of an image-based technique to examine joint congruency at the elbow. *Comput Methods Biomech Biomed Engin*. 2013;16(3):280–290.
20. Buzzell JE, Weikert DR, Watson JT, Lee DH. Precontoured fixed-angle volar distal radius plates: a comparison of anatomic fit. *J Hand Surg Am*. 2008;33(7):1144–1152.
21. Orbay JL, Fernandez DL. Volar fixed-angle plate fixation for unstable distal radius fractures in the elderly patient. *J Hand Surg Am*. 2004;29(1):96–102.
22. Oppermann J, Bredow J, Beyer F, et al. Distal radius: Anatomical morphometric gender characteristics: do anatomical pre-shaped plates pay attention on it? *Arch Orthop Trauma Surg*. 2015;135(1):133–139.